Paper
Int'l J. of Aeronautical & Space Sci. 17(3), 442–453 (2016)
DOI: http://dx.doi.org/10.5139/IJASS.2016.17.3.442

IJASS
International Journal of Aeronautical and Space Sciences

Test and Simulation of an Active Vibration Control System for Helicopter Applications

Do-Hyung Kim* and Tae-Joo Kim**

Rotorcraft Research Team, Korea Aerospace Research Institute, Daejeon 34133, Republic of Korea

Se-Un Jung* and Dong-Il Kwak******

Rotary-Wing Flight Performance Team, Korea Aerospace Industry, Sacheon 52529, Republic of Korea

Abstract

A significant source of vibration in helicopters is the main rotor system, and it is a technical challenge to reduce the vibration in order to ensure the comfort of crew and passengers. Several types of passive devices have been applied to conventional helicopters in order to reduce the vibration. In recent years, helicopter manufacturers have increasingly adopted active vibration control systems (AVCSs) due to their superior performance with lower weight compared with passive devices. AVCSs can also maintain their performance over aircraft configuration and flight condition changes. As part of the development of AVCS software for light civil helicopter (LCH) applications, a test bench is constructed and vibration control tests and simulations are performed in this study. The test bench, which represents the airframe, is excited using a pair of counter rotating force generators (CRFGs) and a multiple input single output (MISO) AVCS that consists of three accelerometer sensors and a pair of CRFGs; a filtered-x least mean square (LMS) algorithm is applied for the vibration reduction. First, the vibration control tests are performed with uniform sensor weights; then, the change in the control performance according to changes in the sensor weight is investigated and compared with the simulation results. It is found that the vibration control performance can be tuned through adjusting the weights of the three sensors, even if only one actuator is used.

Key words: active vibration control system (AVCS), multiple input single output (MISO), counter rotating force generator (CRFG), sensor weight

1. Introduction

The significant sources of helicopter vibration in the cabin are the main rotor, tail rotor, main rotor transmission, and rotating equipment. The vibration induced by these sources, except the main rotor, is usually reduced to acceptable levels through appropriate interventions. An out-of-balance condition on any rotating equipment including the engine, tail rotor drive shaft, hydraulic pump, and electric generator will cause periodic vibrations at a frequency corresponding to the rotating speed of the equipment and its harmonics. Vibration from the rotating equipment is usually minimized through design, precision in manufacturing, and correct maintenance. Similarly, the vibration caused by the meshing of the main rotor transmission gears is also minimized through design and precision in manufacturing. The periodic vibration induced by the tail rotor is composed of frequencies that are integer multiples of the tail rotor's rotational frequency (1/rev). The 1/rev vibration at the rotational frequency is caused by the out-of-balance condition and is typically reduced to acceptable levels through balancing the tail rotor. The other important vibration is at a frequency equal to the rotational frequency (1/rev) multiplied by the number of rotor blades (N). This N/rev vibration is at the "blade-passing frequency". The N/rev vibration is typically minimized through the tail rotor and boom design. Tail rotor-induced vibration is usually

* Senior Research Engineer, Corresponding author: dhkim@kari.re.kr
** Senior Research Engineer
*** Research Engineer
**** Senior Research Engineer

Received: May 2, 2016 Revised: July 28, 2016 Accepted: August 19, 2016

http://ijass.org pISSN: 2093-274x eISSN: 2093-2480

at frequencies several times higher and at amplitudes significantly lower than main rotor-induced vibration. Thus, helicopter designers have traditionally focused on reducing the vibration induced by the main rotor blades.

Like the tail rotor, the periodic vibration induced by the main rotor is composed of frequencies that are integer multiples of the main rotor's rotational frequency. The 1/rev vibration at the rotational frequency is caused by an out-of-balance condition and maintenance to balance the rotor is the typical method of reducing the 1/rev vibration to acceptable levels. The N/rev vibration of the main rotor and vibration at the harmonics of this frequency are of most concern to helicopter designers. The main rotor-induced vibration is unavoidable and inherent to the physics of helicopter flight. The periodic forces and moments on the helicopter result from the combined effect of the varying aerodynamic loads on each blade as it makes a revolution. Vibration can also be caused by downwash from the blades hitting the fuselage. Furthermore, changing the flight regimes changes the aerodynamic loads, which means that the N/rev vibration is not steady across an entire flight region. Moreover, changes in the rotor speed result in changes in the base frequency of the main rotor-induced vibration.

There are numerous potential negative effects of helicopter vibration, including passenger discomfort, crew fatigue and increased task difficulty, reduced airframe fatigue life, reduced flight envelope, lower equipment reliability, more hydraulic leaks, increased life-cycle costs, and so on. Therefore, reducing helicopter vibration is beneficial to a broad spectrum of performance, reliability, life, and cost measures. To date, numerous approaches to reducing vibration have been explored and developed. These approaches fall into two broad categories: passive and active approaches. Passive vibration control seeks to reduce helicopter vibration through generating counter-vibration forces (absorption) or motion (isolation) without power input. Active vibration control seeks to reduce helicopter vibration using electric and/or hydraulic power to generate controllable counter-vibration forces (cancellation). Passive approaches appeared first because active approaches were not practical. Typical passive devices are rotor head-mounted vibration absorbers, compliant mounts (isolators), and airframe-mounted vibration absorbers. Passive approaches are limited by the frequency range over which the vibration control is effective. The designs must be optimized for the periodic vibration frequency of interest, typically N/rev. Vibration control becomes significantly less effective whenever the rotor speed deviates from the nominal speed; under such flight conditions, the rotor-induced vibration levels will increase. Performance penalties are incurred with these approaches: weight and drag, which increases for rotor head-mounted absorbers. However, active approaches are capable of eliminating or reducing these limitations and costs.

Advances in technology over the past few decades have enabled practical active vibration control systems (AVCSs) to be developed for aircraft: hardware and software technologies for embedded systems, control algorithms, force generators, and piezoelectric sensors. The first active approaches developed followed the same logic that was pursued with the passive approaches: reduce the vibration at its source, i.e. the main rotor. Higher Harmonic Control (HHC) modulates the pitch of the main rotor blades using the flight-critical swash-plate hydraulic actuators to reduce the oscillatory loads that cause vibration [1, 2]. This approach works, but it has not been adopted due to the excessive amount of hydraulic power required and airworthiness concerns with using safety-critical actuators. Several active approaches that directly control the main rotor blade response have also been explored and developed. Active trailing edge flap demonstrated its capability for vibration reduction in wind tunnels and flight tests [3-6], but it has not been approved as being airworthy. The active twist [7-10] and active tab [11-13] approaches have also demonstrated potential, but their technologies have not matured for flyable devices.

The next approach developed was an active/adaptive system that "cancels" the rotor-induced airframe vibration. The Active Control of Structural Response (ACSR) system was initially developed by Westland Helicopters for the W-30 helicopter in the late 1980s [14]. Since the 1990s, AVCSs incorporating accelerometers and force generators composed of electric motors and eccentric masses became commercially available, and they have been applied to several helicopters including the S-92, V-22, UH-60M, S-76D, AW139, and EC225/725. These active/adaptive approaches proved effective over a range of helicopter frequencies and configurations, and they have resulted in significantly lower rotor-induced vibration beyond what was achievable with passive approaches [15].

The first Korean Utility Helicopter, SURION, adopted several passive devices in addition to the structural design optimization in order to minimize vibration in the cabin [16]. However, the Medical Evacuation (MEDEVAC) version, a variant of SURION, is under development incorporating AVCS, which is being provided by a foreign company in order to achieve the required vibration level with a lower weight compared with that using passive devices. Now, Korea Aerospace Research Institute (KARI) and Korea Aerospace Industry (KAI) are jointly developing AVCS software for light

civil helicopter (LCH) applications. A test environment was prepared in order to investigate the vibration control algorithm. The test system consists of a bench representing the airframe, controllable force generating actuators, accelerometers, and a rapid control prototyping (RCP) system for real-time control algorithm application. The test bench was constructed, and a multiple input single output (MISO) control algorithm was applied with various sensor weights. The control performance according to the sensor weight changes was investigated and compared with the simulation results. This paper focuses on investigating the capability of tuning the vibration control performance at multiple locations with a single actuator and the variations of the control commands with respect to the sensor weight changes.

2. Test Setup

2.1 Test Bench and RCP System

The test bench was constructed to represent an airframe cabin structure. While it would be better to use a real airframe structure as the test bench in order to provide more meaningful information for selecting sensor and actuator locations, this was not achievable due to cost and time restraints. However, if realistic vibration levels are induced at the same N/rev frequency in the simple test bench, it can provide meaningful information during the algorithm development. Furthermore, utilizing a simple test bench is more cost effective. The specifications of the test bench are outlined in Table 1, and the configuration is depicted in Fig. 1. The main frame is composed of two I-beams in the longitudinal direction and three U-shaped beams are reinforced in the lateral direction. In order to simplify the bench motion, four suspension systems were applied under the bench. The force generator can be placed in thirteen different locations in order to excite the structure and control the induced vibration. Furthermore, fourteen locations were prepared for the accelerometer installation.

Table 1. Specifications of the test bench.

Property	Value
Width	1,600 mm
Length	2,460 mm
Height	900 mm
Weight	200 kg
CRFG locations	13
Accelerometer locations	14
Suspension	Coil spring
Material	Aluminum

In this study, the front region of the bench was selected as the target area for the vibration control, so three accelerometers (Acc2, Acc3, and Acc4) were used as the control accelerometers. Vibration was generated using a pair of counter rotating force generators (CRFG1) located in the center of the bench, and another pair of CRFGs (CRFG2) were installed under the right seat below Acc3 as the control actuator. A dummy weight of 250 kg was distributed on top of the bench in order to provide pre-strain to the suspension springs for a smooth motion. The number of actuators available for the test bench was two pairs; thus, one pair was used for the exciting vibration and the other pair was used for the control actuator. The numbers and locations of the sensors were not optimized in this study: the optimization

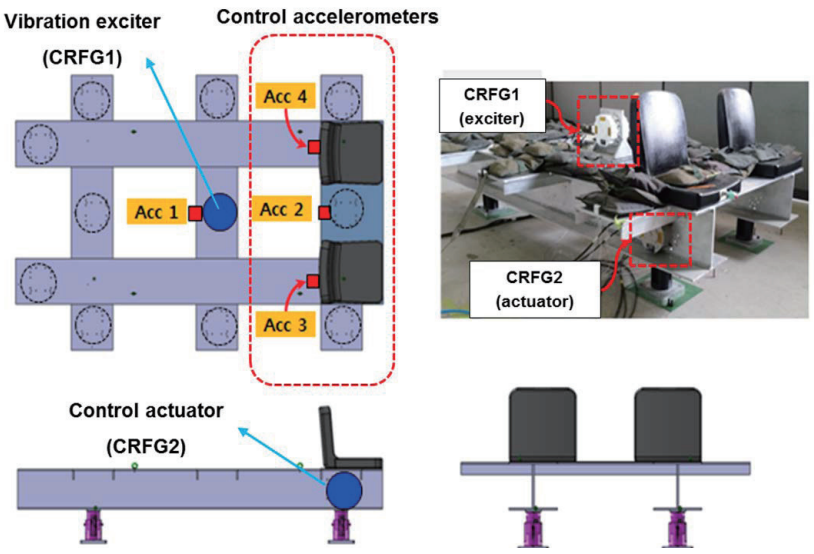

Fig. 1. Configuration of the test bench.

of the numbers and locations of actuators can be found in previous work [17].

The control algorithm was modeled using MATLAB/Simulink [18], and it was implemented in real-time on a DS1006 processor board-based RCP system of dSPACE. The overall test setup is depicted in Fig. 2. The control algorithm model was compiled in the host PC and downloaded to the RCP system. The real-time operating software was also running on the host PC in order to monitor signals, modify parameters, and save data. The ICP accelerometer sensor signals were connected to the A/D module through the signal conditioner, and the calculated control command was sent to the force generator controller (FGC) using an RS-422 serial interface. The FGC was powered by 115 VAC, 400 Hz, 3-phase power supply, and it sent electric signals to operate the brushless motors of CRFGs.

2.2 Control Actuator

The force generator (FG) or actuator is a key element in AVCSs in order to generate controllable counter-vibration forces. The currently available off-the-shelf force generators are single-point actuators that apply inertial forces to the airframe at their attached points. There are two main types of inertial force generator that are differentiated by how the inertia is moved to generate force: rotating inertia and oscillating inertia. The rotating inertia FG is based on the principle of generating inertial forces through rotating an eccentric mass to generate rotary force; the oscillating inertia FG is based on the principle of generating inertia force through oscillating a mass to generate a linear force.

Moog Inc.'s CRFGs [19] are used in this study. CRFG-based AVCSs have been used in several aircraft including the S-92, UH-60M, and V-22. One CRFG employs two eccentric masses rotated in opposite directions (counter-rotated) using a single electric motor and associated gear system. The counter-rotating masses in one CRFG produce a sinusoidal inertial force along a single axis, as depicted in the force vector diagram in Fig. 3. The force amplitude is proportional to the square of the rotational frequency. For a given rotational frequency, the amplitude of the force generated is fixed for a single CRFG. Control of the relative phase between a pair of CRFGs enables the combined sinusoidal force amplitude and phase to be controlled. The configuration of

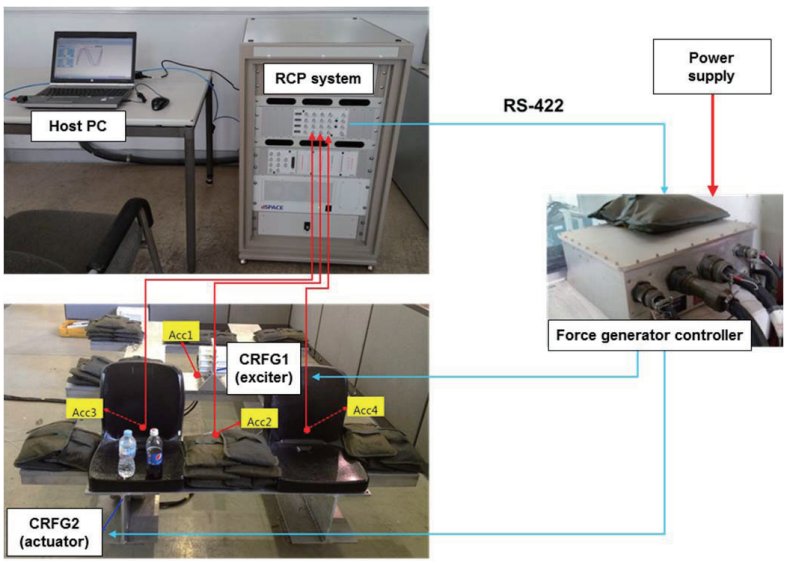

Fig. 2. Test setup.

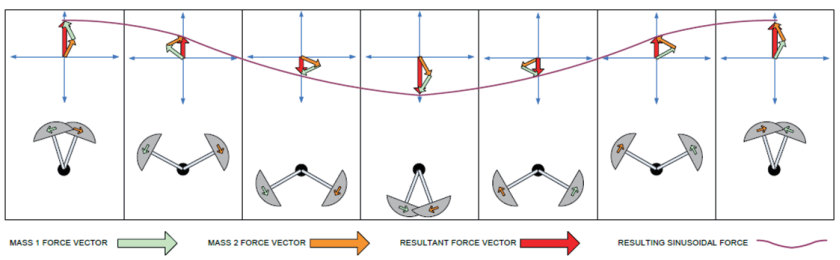

Fig. 3. Force vector diagram of a CRFG, Moog Inc.

the CRFG and schematic of a rotating eccentric mass in a pair of CRFGs are depicted in Fig. 4. Two pairs of CRFGs are installed in the test bench in order to generate disturbance and control force. The key features are listed in Table 2. The weight increase of the test bench resulting from the use of the CRFGs can be considered large; however, AVCSs typically exhibit superior performance with lower weight compared with conventional passive vibration absorbers.

Table 2. Specifications of the CRFGs.

Model	Property	Value
CRFG1 (exciter pair)	Max. force	5,398 N @ 18.0 Hz
	Operating range	14.7~23.5 Hz
	Weight	14.6 kg
CRFG2 (actuator pair)	Max. force	1,484 N @ 18.0 Hz
	Operating range	14.7~23.5 Hz
	Weight	8.7 kg

3. Real-time Vibration Control

3.1 Control Algorithm

The AVCS is designed to cancel the largest amplitude in the cabin structure, which is the N/rev component. The N/rev frequency can change during flight, but the variation in the rotor speed is narrow. Therefore, a filtered-x least mean

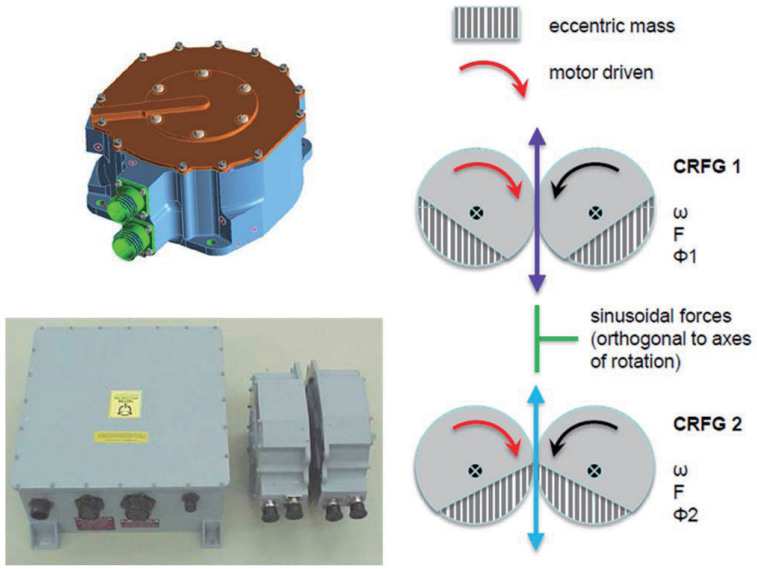

Fig. 4. Pairing two CRFGs, Moog Inc.

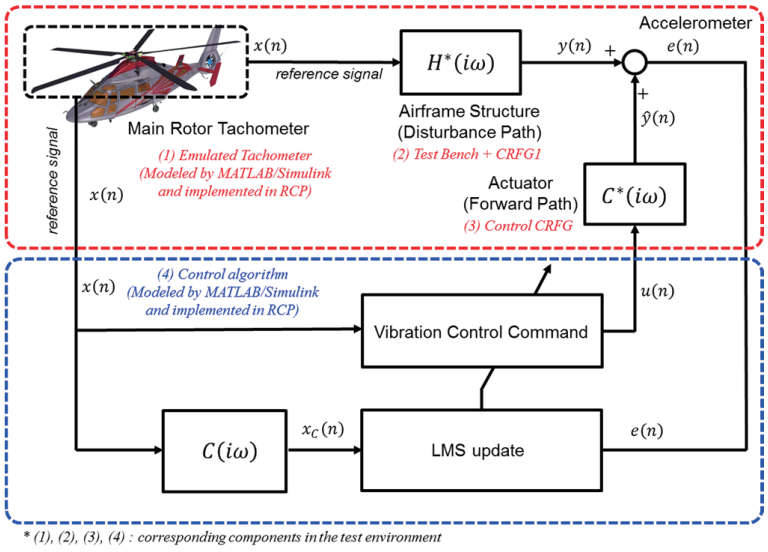

Fig. 5. Architecture of the AVCS and FxLMS algorithm.

square (FxLMS) feedforward algorithm [20, 21] was adopted in this study because it is robust, easy to implement, and very relevant for tonal disturbances. The architecture of the FxLMS algorithm is depicted in the lower part of Fig. 5. The upper part of Fig. 5 represents the plant model (disturbance path) H^* and the actuator model (forward path) C^*. The control algorithm calculates the control command $u(n)$ using the reference input $x(n)$ generated by the tachometer and the error signal $e(n)$ measured by the accelerometers. The control command is fed into the actuator and then the secondary vibration $\hat{y}(n)$ is generated to cancel the primary vibration $y(n)$. C^* represents the transfer function of the forward path or secondary path dynamics, from the control command to the generated secondary vibration. C is the numerical model of C^* identified through testing.

The error signal is the sum of the primary vibration induced by the main rotor and the secondary vibration produced by the actuator. It can be expressed as follows:

$$e(n) = y(n) + \hat{y}(\mathrm{n}) = y(n) + C^* u(n) \tag{1}$$

Vibration control minimizes the error signal. The cost function can be defined as follows:

$$J = E\{|e(n)|^2\} = e(n)^H e(n) \tag{2}$$

where $e(n)^H$ is the conjugate transpose of $e(n)$. The cost function is a function of $u(n)$ for a given disturbance $y(n)$, and a positive quadratic form shaped like a basin. The optimal control input for an unconstrained force can be calculated as follows if there are more sensors than actuators:

$$u_{opt} = -(C^H C^*)^{-1} C^H y \tag{3}$$

It is not worthwhile to compute the optimal solution constantly because the disturbance $y(n)$ is changing and it is a costly operation. Furthermore, the disturbance $y(n)$ is not directly accessible or measurable due to the presence of vibration from the actuator forces. Therefore, the steepest descent algorithm is applied to iteratively adjust the control command to go in the direction that minimizes the cost function.

$$u(n+1) = u(n) - \frac{\mu}{2} \nabla J \tag{4}$$

where μ is the rate of convergence, which must be selected in order to allow a good compromise between reactivity and stability. The number of sensors should be larger than the number of FGs in order to prevent ill-conditioning and slow convergence. It is called the FxLMS because the reference signal is filtered and combined with C to compute ∇J. It produces a harmonic command at a frequency given by the reference. After some math to calculate the gradient of the cost function, equation (4) can be expressed as follows:

$$u(n+1) = u(n) - \mu C^{*H} e(n) \tag{5}$$

In practice, the estimated system model C is used for the forward path dynamics C^*.

$$u(n+1) = u(n) - \mu C^H e(n) \tag{6}$$

This equation is called the update equation. For practical implementation, the accelerometer weighting can be adjusted through introducing diagonal weight matrix Q. The cost function and update equation are revised as follows:

$$J = e(n)^H Q e(n) \tag{7}$$

$$u(n+1) = u(n) - \mu C^H Q e(n) \tag{8}$$

The vibration cancellation trade-off between the accelerometers can be obtained through tuning the weight values. The update equation (8) is modeled using Simulink for real-time vibration control experiment.

3.2 Test Cases and Simulations

In order to implement the FxLMS algorithm, the forward path dynamics, which is the transfer function of CRFG2 in this study, should be identified. The forward path dynamics are assumed to be linear time invariant (LTI), and the relationship between the output responses induced by known command input are identified. For a specific sinusoidal input to a LTI system with a fixed frequency, the output response is changed in terms of magnitude and phase with the same frequency. The excitation frequency was set to 18 Hz, which is the same condition of four-bladed rotor system with 270 rpm rotating speed. The forward path model was assumed to be $C(i\omega)=A_C\text{-}iB_C$, and the LMS method was applied in order to minimize the error between the actual forward path and the numerical model, as depicted in Fig. 6. The obtained system model, C, was used in the control algorithm.

For vibration control experiment, the disturbance was

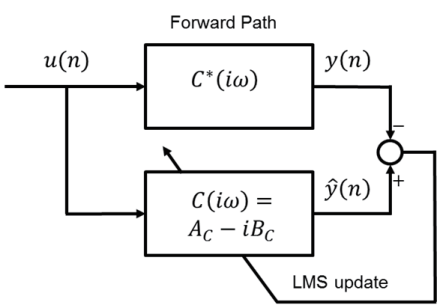

Fig. 6. Forward path system identification.

generated by CRFG1 using a sinusoidal wave with an 18 Hz frequency. The amplitude of the disturbance command was increased from zero to a certain value that induces approximately 0.3~0.4 g vibration at accelerometers Acc2, Acc3, and Acc4; then, the disturbance condition was fixed. The same reference signal emulating tachometer was fed into the FxLMS algorithm in order to generate the control command. Steady and transient vibration control performances with various sensor weights were measured. The test cases are listed in Table 3. For all cases, the vibration disturbance condition was the same as described above. Case 1 is the baseline case with the control actuator "off". Case 2 is the idle condition with the actuator spinning but generating zero force. Case 3 is the uniform weight case with the weight vector for Acc2, Acc3, and Acc4 being [1 1 1]. Cases 4 to 15 are generated through changing the weight of each sensor. When the sensor weights were changed, the magnitude of the weight vector, $\sqrt{w_{Acc2}^2 + w_{Acc3}^2 + w_{Acc4}^2}$ was maintained, i.e. $\sqrt{3}$. Cases 4, 5, and 6 are when one of three sensors had an increased weight value of 1.2 and the others were decreased in order to maintain the norm of the weight vector. Cases 7–9, cases 10–12, and cases 13–15 are when one of the three sensors had weight increases of 1.4, 1.6, and 1.7, respectively. Case 16 was prepared in order to investigate the transient performance with the control algorithm turned "on" from the "off" state. During the vibration control test, the magnitude of the control command was limited to 60% of the maximum force at 18 Hz in order to prevent excessive force being applied to the test bench.

Table 3. Test cases

ID	Weighting [Acc2 Acc3 Acc4]			CRFG1 (exciter)	CRFG2 (actuator)	Remark
1	0	0	0	on	off	Baseline
2	0	0	0	on	on	Idle
3	1.00	1.00	1.00	on	on	
4	1.20	0.88	0.88	on	on	
5	0.88	1.20	0.88	on	on	
6	0.88	0.88	1.20	on	on	
7	1.40	0.72	0.72	on	on	
8	0.72	1.40	0.72	on	on	
9	0.72	0.72	1.40	on	on	steady
10	1.60	0.47	0.47	on	on	
11	0.47	1.60	0.47	on	on	
12	0.47	0.47	1.60	on	on	
13	1.70	0.23	0.23	on	on	
14	0.23	1.70	0.23	on	on	
15	0.23	0.23	1.70	on	on	
16	1.00	1.00	1.00	on	off → on	transient

In order to investigate the characteristics of the entire system, simulations were also performed. The hardware part of the system in Fig. 5 was modeled. The forward path model was already identified for the implementation of the FxLMS algorithm. One more numerical model for the plant should be identified. The disturbance path model, i.e. the transfer function of the test bench, was identified using the same procedure for the forward path system identification. The disturbance path model was also assumed to be linear time invariant, and the relationship between the output responses induced by the known command input for CRFG1 were identified using a test. The same frequency (18 Hz) was used for the excitation. The disturbance path model was assumed to be $H(i\omega)=A_H\text{-}iB_H$, and the LMS method was applied in order to minimize the error between the actual disturbance path dynamics and the numerical model output. The obtained $H(i\omega)$ and $C(i\omega)$ were used in the MATLAB/Simulink model, and the same cases listed in Table 3 were simulated.

4. Results and Discussion

4.1 Control Performance

First, the vibration levels without the control were Acc2 = 0.301 g, Acc3 = 0.332 g, and Acc4 = 0.393 g. When the vibration control algorithm with uniform weights was turned "on", the vibration amplitudes at the three locations were reduced by 67.0%, 74.6%, and 13.6%, respectively. The vibration control performance changed according to the sensor weights. The steady vibration amplitudes of the test cases are summarized in Table 4. For clear understanding of the effects of the weight changes on the steady performance, the Acc2 weight increase cases are compared in Fig. 7. As the weight of Acc2 increased, the vibration amplitude of Acc2 decreased. However, the amplitude of Acc3 increased because the weight of Acc3 decreased. The same trend was captured in the simulations. Figures 8 and 9 are the results for the Acc3 and Acc4 weight increase cases, respectively. The same trend in the performance changes were found in the tests and simulations. For the same increments of sensor weight, Acc3 exhibited excellent performance enhancement, but the effect of the weight increase at Acc4 was slight. The location of Acc3 was above the actuator and Acc4 was the farthest

Table 4. Steady vibration amplitude

Test ID	Acc2 (g)	Acc3 (g)	Acc4 (g)
1	0.301	0.332	0.393
2	0.298	0.337	0.402
3	0.107	0.082	0.346
4	0.099	0.084	0.339
5	0.112	0.066	0.347
6	0.115	0.093	0.337
7	0.084	0.099	0.337
8	0.116	0.047	0.346
9	0.126	0.129	0.334
10	0.071	0.120	0.338
11	0.121	0.025	0.348
12	0.142	0.166	0.327
13	0.047	0.141	0.344
14	0.131	0.014	0.354
15	0.193	0.213	0.327

from the actuator. Therefore, it can be understood that the actuator has more control authority for closer locations in the current AVCS configuration.

The transient performance was also explored during the test. The AVCS controller was turned "on" from the "off" state during test case 16. Figure 10 presents the time history of the accelerometers for test case 16. The controller was turned "on" at t = 8 sec. The vibration amplitude decreased and converged to a steady state within 2 sec. The simulation result demonstrates very similar behavior. The settling time can be adjusted through changing the convergence rate μ, but fixed values were used in this study.

4.2 Control Command

The control command calculated using equation (8) is sinusoidal, and it can be decomposed into cosine and sine components. The trajectories of the control command for case 16, i.e. uniform weight, are depicted in Fig. 11. The

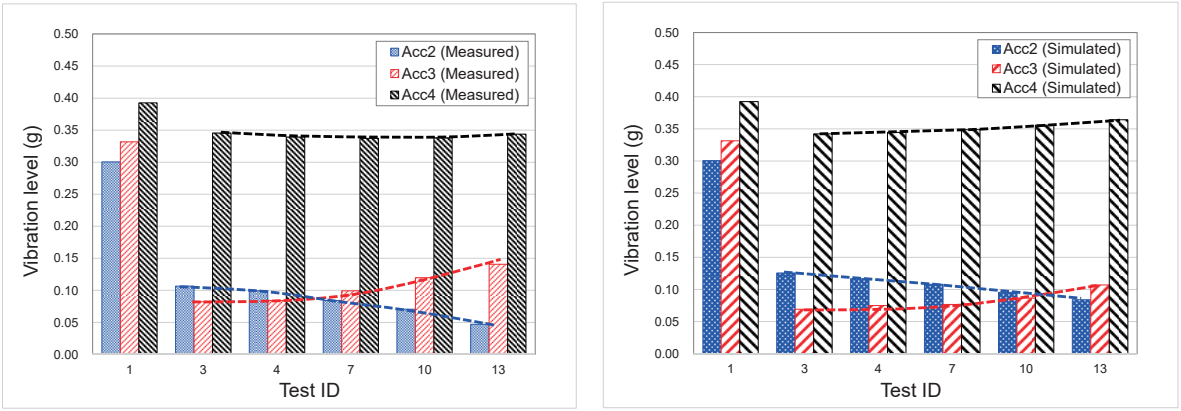

(a) Test results. (b) Simulation results.

Fig. 7. Vibration control performance with respect to the Acc2 weight increases.

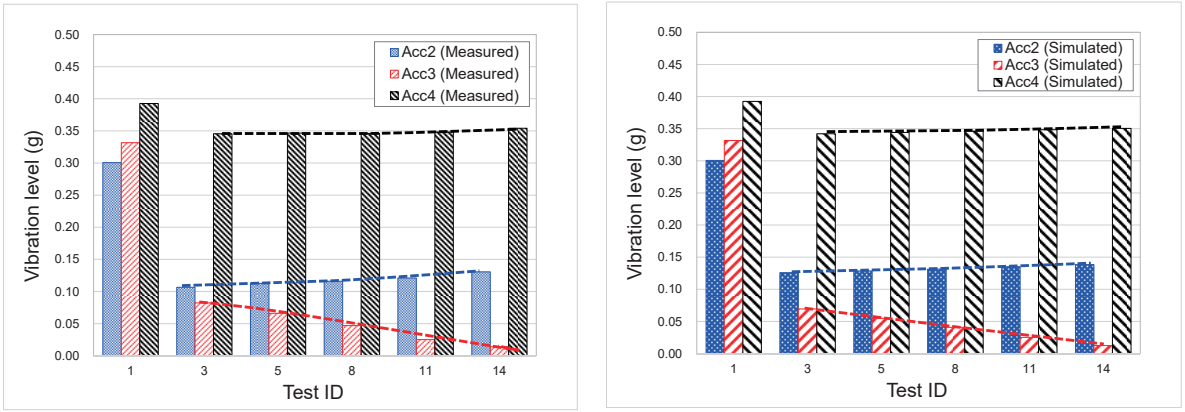

(a) Test results. (b) Simulation results.

Fig. 8. Vibration control performance with respect to the Acc3 weight increases.

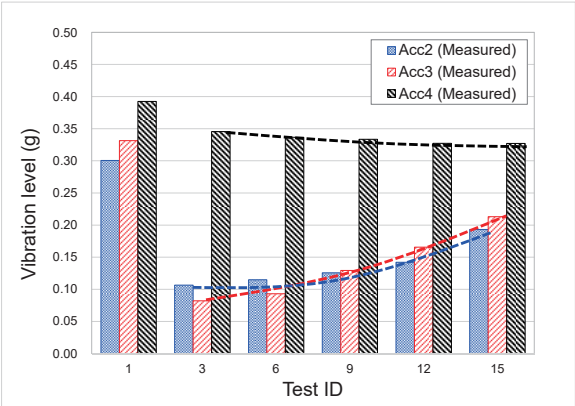

(a) Test results.

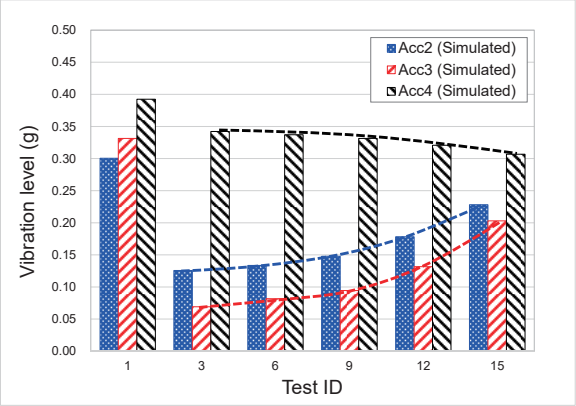

(b) Simulation results.

Fig. 9. Vibration control performance with respect to the Acc4 weight increases.

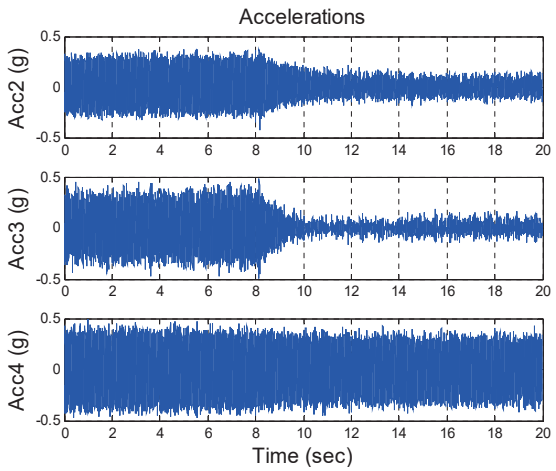

(a) Test results.

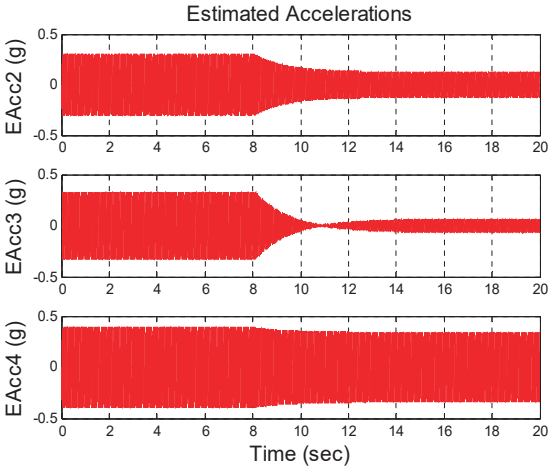

(b) Simulation results.

Fig. 10. Transient vibration control performance.

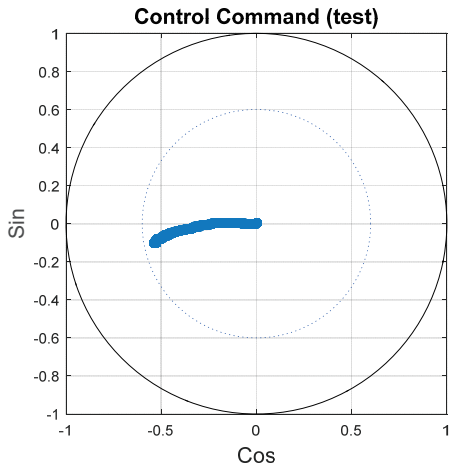

(a) Test results.

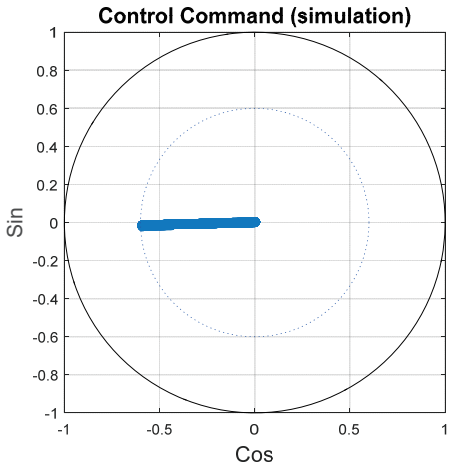

(b) Simulation results.

Fig. 11. Trajectory of the control command.

DOI: http://dx.doi.org/10.5139/IJASS.2016.17.3.442

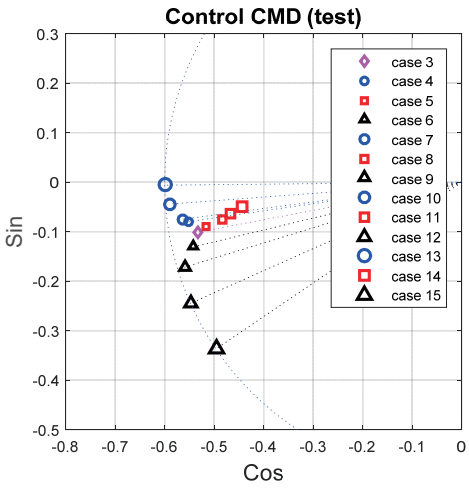

(a) Test results.

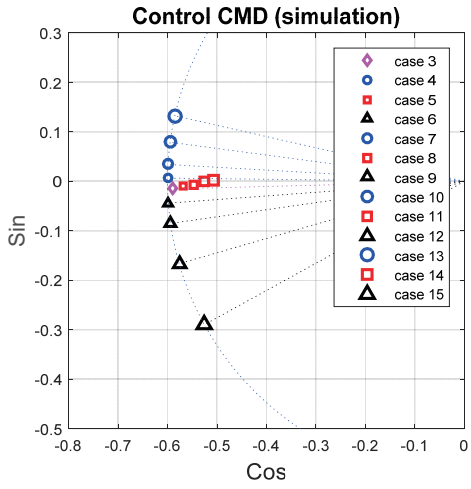

(b) Simulation results.

Fig. 12. Control command variations with respect to the weight changes.

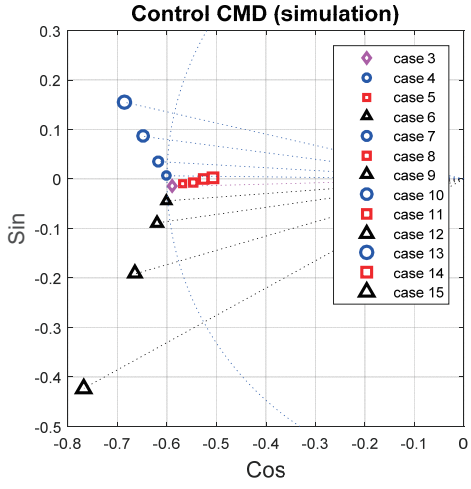

Fig. 13. Simulated control command with the 100% force limit.

x-axis and y-axis represent the cosine and sine components of the control command, respectively. The magnitude is normalized by the maximum force at 18 Hz. The outer circle is the 100% force command boundary and the inner circle is the 60% force limitation used in the test for safe operation. The initial condition was set to (0, 0). It can be seen that the control command began from the center of the graph, then moved to the left, and finally converged within the 60% force limit boundary. The simulated trajectory was a straight line, but the test result was a slightly curved line. For the control system modeling, it was assumed that the forward path and disturbance path models were LTI. However, the actual system has nonlinearity with respect to changes in the frequency and/or the amplitude of excitation, and there can be a modeling error, which produces a curved command trajectory. However, it is well known that convergence is guaranteed if the phase between C and C^* is between ±90° [22]. Thus, a small amount of estimation error in the forward path is not severe.

The variations in the steady state control command with respect to the sensor weight changes are presented in Fig. 12. Due to the force magnitude limitation, the control command could not go further, but the directional changes are traceable. The directional changes for the weighting of each accelerometer was almost evenly spaced in the solution plane. This is more clearly seen in Fig. 13, which depicts the simulated results with 100% force magnitude limitation. Increasing the weight of Acc2 moves the optimal solution toward the upper left; additional weight in Acc3 moves it slightly toward the upper left; and the solution moves to the lower left corner for the Acc4 cases. Regarding the magnitude change of the control command, it can be seen that increasing the weight of Acc4 requires significantly more force and increasing the weight of Acc3 requires less force than the baseline case. Therefore, it can be seen again that the actuator has more control authority for closer locations in the current AVCS configuration.

5. Conclusion

An AVCS test bench was constructed to test a control algorithm for helicopter applications and an FxLMS-based algorithm was implemented for real-time vibration control. The capability of tuning the vibration control performance at three locations with one actuator and the variations of the control command with respect to the sensor weight changes were investigated using tests, and the test results were compared with the simulation results.

The test results demonstrated that enhanced vibration

control performance could be obtained at a specific location through increasing the weight of the sensor at that location. However, it also produced a negative effect at the other sensor locations. The vibration amplitude increased at the other locations due to the relatively decreased sensor weights. Furthermore, the same results were obtained in the simulations, so the prediction of the dynamic behavior appears practical. The test and simulation results demonstrated that adjusting the vibration control performance at multiple locations with one actuator and multiple sensors is possible through adjusting the sensor weights.

The control command variations according to the sensor weight changes exhibited very similar characteristics found in the tests and simulations. The trajectories of the control command changes with increasing sensor weights of one of the three sensors were almost evenly spaced along the solution plane. Furthermore, increasing the closest sensor weight resulted in decreased control effort and more control force must be supplied if the weight of the farthest sensor is increased. That is, the control authority is highly related to the distance between the sensors and the actuator.

Acknowledgement

This study was conducted for the LCH Development Program (Project Number: 10053157) funded by the Ministry of Trade, Industry and Energy (Korea).

References

[1] Gmelin, B., Heller, H., Philippe, J. J., Mercker, E. and Preisser, J. S., "HHC Aeroacoustics Rotor Test at the DNW: The Joint German/French/US HART Project", *20th European Rotorcraft Forum*, Amsterdam, Netherlands, October 1994, Paper 115.

[2] Gmelin, B. L., Heller, H., Mercker, E., Philippe, J. J., Preisser, J.S. and Yu, Y. H., "The HART Programme: A Quadrilateral Cooperative Research Effort", *51st Annual Forum of the American Helicopter Society*, Fort Worth, TX, May 1995, pp. 695-709.

[3] Roth, D., Enenkl, B. and Dieterich, O., "Active Rotor Control by Flaps for Vibration Reduction – Full scale demonstrator and first flight test results", *32nd European Rotorcraft Forum*, Maastricht, The Netherlands, 2006.

[4] Straub, F. and Anand, V., "Aeromechanics of the SMART Active Flap Rotor", *63rd Annual Forum of American Helicopter Society*, Virginia Beach, VA, May 1-3, 2007.

[5] Kobiki, N. and Saito, S., "Performance Evaluation of Full Scale On-board Active Flap System in Transonic Wind Tunnel", *64th Annual Forum of American Helicopter Society*, Montreal, Canada, April 29-May 1, 2008.

[6] Lorber, P., O'Neil, J., Isabella, B., Andrews, J., Brigley, M., Wong, J. and LeMasurier, P., "Whirl and Wind Tunnel Testing of the Sikorsky Active Flap Demonstration Rotor", *67th Annual Forum of American Helicopter Society*, Virginia Beach, VA, May 3-5, 2011.

[7] Bernhard, A. and Wong, J., "Sikorsky Active Rotor Control Evaluation of NASA/Army/MIT Active Twist Rotor", *59th Annual Forum of American Helicopter Society*, Phoenix, Arizona, May 6-8, 2003.

[8] Weems, D., Anderson, D., Mathew, M. and Bussom, R., "A Large-Scale Active-Twist Rotor", *60th Annual Forum of American Helicopter Society*, Baltimore, MD, June 7-10, 2004.

[9] Wierach, P., Riemenschneider, J., Optiz, S. and Hoffmann, F., "Experimental Investigation of an Active Twist Model Rotor Blade under Centrifugal Loads", *33rd European Rotorcraft Forum*, Kazan, Russia, September 11-13, 2007.

[10] Lim, J. W., Boyd Jr., D. D., Hoffmann, F., van der Wall, B. G., Kim, D. H., Jung, S. N., You, Y. H., Tanabe, Y., Bailly, J., Lienard, C. and Delriuex, Y., "Aeromechanical Evaluation of Smart- Twisting Active Rotor", *40th European Rotorcraft Forum*, Southampton, UK, September 2-5, 2014.

[11] Kobiki, N., Saito, S., Akasaka, T., Tanabe, Y. and Fuse, H., "An Experimental Study for Aerodynamic and Acoustic Effects of On-blade Active Tab", *31st European Rotorcraft Forum*, Italy, September 2005.

[12] Kim, D. H., Kang, H. J., Wie, S. Y. and Kim, S. H., "Modeling of a Rotor System Incorporating Active Tab and Analysis of BVI Noise Reduction Characteristics", *Journal of the Korean Society for Aeronautical and Space Sciences*, Vol. 41, No. 11, 2013, pp. 855-864.

[13] Kobiki, N., Tanabe, Y., Aoyama, T., Kim, D. H., Kang, H. J., Wie, S. Y. and Kim, S. H., "Design, Analysis and Prototyping of Active Tab Rotor", *41st European Rotorcraft Forum*, Munich, Germany, September 1-4, 2015.

[14] Staple, A. E., "An Evaluation of Active Control of Structural Response as a Means of Reducing Helicopter Vibration", *Proceedings of the 46th Annual Forum of the American Helicopter Society*, Washington, DC, May 21-23, 1990.

[15] Swanson, D., Black, P., Girondin, V., Bachmeyer, P. and Jolly, M., "Active Vibration Control Using Circular Force Generators", *41st European Rotorcraft Forum*, Munich, Germany, September 1-4, 2015.

[16] Jung, S. U., Kwak, D. I., Kim, S. H., Choi, J. H. and Shin, D. S., "Vibration Reduction Devices for Korean Utility Helicopter", *Journal of the Korean Society for Aeronautical and Space Science*s, Vol. 41, No. 12, 2013, pp. 987-993.

[17] Kim, D. H., Kim, T. J, Paek, S. K., Kwak, D. I. and Jung, S. U., "Application and Performance Evaluation of Helicopter Active Vibration Control System for Surion", *Journal of the Korean Society for Aeronautical and Space Sciences*, Vol. 43, No. 6, 2015, pp. 557-567.

[18] *Simulink User's Guide*, The Mathworks Inc., Natrick, MA, 2015.

[19] Garnjost, K. D. and Rey, G. J. (Moog Inc, USA). *Modular vibratory force generator, and method of operating same*, US Patent 5,903,077, May 11, 1999.

[20] Elliott, S. J. and Nelson, P. A., "Active Noise Control", *IEEE Signal Processing Magazine*, pp. 12~35, October 1993.

[21] Kamenetsky, M. and Widrow, B., "A Variable Leaky Adaptive Algorithm", *38th Asilomar Conference on Signals, Systems and Computers*, Pacific Grove, CA, Nov. 7-10, 2004.

[22] Elliott, S. J., Stothers, I. M. and Nelson, P. A., "A Multiple Error LMS Algorithm and its Application to the Active Control of Sound and Vibration", *IEEE Transactions on Acoustics, Speech, and Signal Processing*, Vol. ASSP-35, No. 10, 1987, pp. 1423–1434.